JACS
JOURNAL OF THE AMERICAN CHEMICAL SOCIETY

Communication

pubs.acs.org/JACS

Terazulene: A High-Performance n-Type Organic Field-Effect Transistor Based on Molecular Orbital Distribution Control

Yuji Yamaguchi, Keisuke Ogawa, Ken-ichi Nakayama,* Yoshihiro Ohba, and Hiroshi Katagiri*

Graduate School of Science and Engineering, Yamagata University, 4-3-16 Jonan, Yonezawa, Yamagata, 992-8510, Japan

Supporting Information

ABSTRACT: We present herein a linear expanded π-conjugation system comprising azulene units: **2,6′:2′,6″-terazulene**. This simple hydrocarbon exhibits excellent n-type transistor performance with an electron mobility of up to 0.29 $cm^2 V^{-1} s^{-1}$. The lowest unoccupied molecular orbital (LUMO) is well distributed over the entire molecule, whereas the highest occupied molecular orbital (HOMO) is localized at one end. These findings indicate a disadvantage of hole carrier transport and an advantage of n-type-specific transport behavior. This system presents an unconventional concept: polarity control of OFET by molecular orbital distribution control.

Azulene, a nonalternant hydrocarbon, is a simple aromatic compound with a large dipole moment of 1.08 D.[1,2] A fundamental difference between it and the alternant hydrocarbon naphthalene is that the highest occupied molecular orbital (HOMO) and the lowest unoccupied molecular orbital (LUMO) are not mirror-related in orbital geometry. The absolute values of their atomic orbital coefficients differ substantially, and therefore the energy gap is smaller than anticipated, resulting in a lower transition energy.[2] Since the introduction of the azulene unit can be used to trigger the polarized nature of the ground state or construction of π-conjugated materials with narrow energy gaps, it is hardly surprising that the azulene-based π-conjugation system is likely to propel the development of useful materials in various research areas; examples include conducting polymers,[3,4] electrochromic materials,[5,6] fluorescence switching materials,[7] and anion receptors.[8] Moreover, there are only a few examples that involve the application of azulenes as near-infrared resonance materials: azulene-fused porphyrin,[9] squarylium,[10] and azulenocyanine.[11] OFET is one of the most attractive applications of the highly π-extended aromatic compounds,[12] and recently, we reported 2-azulenyl end-capped oligomers as p-type OFET materials with comparatively high carrier mobilities.[13] A structural expansion at the 2-position of azulene rings led to flat and linear molecular shapes, and the effective π-conjugation system contributed to the development of useful properties in the semiconductor molecules: herringbone orientation and narrow energy gap. We describe herein a simple hydrocarbon compound, **2,6′:2′,6″-terazulene**, wherein three azulene units are connected linearly in the same direction. This molecule has the potential to enhance the unique properties of the azulene unit, including the internal dipole moment and the different distribution of HOMO and LUMO, derived from the nonalternant hydrocarbon character.

The synthetic route of **2,6′:2′,6″-terazulene** is shown in Scheme 1. The chlorination of **1**[14] was performed via a Sandmeyer reaction using isoamyl nitrite, which afforded 2-chloroazulene-6-boronic acid ester **2**. This novel compound is a valuable synthetic intermediate for selective substitution at the 2- and 6- positions in the azulene moiety. Suzuki–Miyaura cross-coupling of **2** with 2-iodoazulene **3**[15,16] proceeded to give chloro-2,6′-biazulene derivative **4**. It was then treated with 100% phosphoric acid to afford **5**. Finally, Suzuki–Miyaura cross-coupling reaction of **5** with 6-azulenyl boronic acid ester **6**[17] gave **2,6′:2′,6″-terazulene** as dark-green crystals. Due to its poor solubility in common solvents, the terazulene was purified by gradient sublimation. It was then characterized by elemental analysis and single-crystal X-ray analysis. Thermogravimetric analysis (TGA) demonstrated that the thermal stability of **2,6′:2′,6″-terazulene** (onset at 440 °C) was higher than that of hexacene (onset at 385 °C)[18] (Figure S19 in Supporting Information [SI]). Since mass loss was not observed until ∼440 °C, thermal decomposition of the azulene skeleton is likely not to have occurred below 440 °C.

Scheme 1. Synthesis of 2,6′:2′,6″-Terazulene

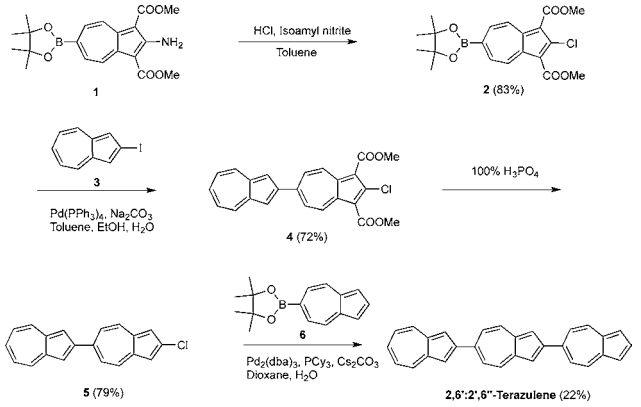

The UV–vis spectra of **2,6′:2′,6″-terazulene** in thin-film form and in *o*-dichlorobenzene (ODCB) solution were recorded (Figure 1A). The azulene molecule showed a strong absorption band at 341 nm, derived from π–π* transition, and a weak absorption band around 580 nm, derived from the unique electronic state of the azulene unit.[2] On the other hand,

Received: October 19, 2013
Published: December 12, 2013

dx.doi.org/10.1021/ja410696j | J. Am. Chem. Soc. 2013, 135, 19095–19098

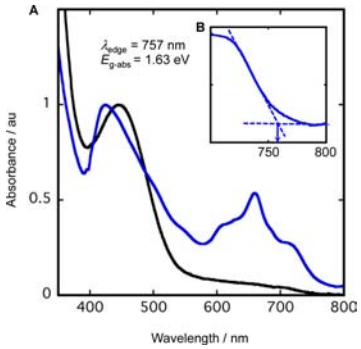

Figure 1. (A) Absorption spectra of 2,6′:2′,6″-terazulene in thin-film form (blue), and in ODCB (black). Inset (B) The lowest transition energies ($E_{g\text{-}abs}$) were determined at the intersection of the line tangent to the long wavelength side of the band and the corrected baseline.

in **2,6′:2′,6″-terazulene**, the former peak exhibited a red-shift to 424 nm, and absorption strengthened in the long-wavelength region around 650 nm. These results indicate that π-conjugation can be extended even in oligoazulene systems when connected at the 2- and 6- positions. Interestingly, the absorption peak due to the electronic state of azulene around 650 nm is markedly enhanced in the thin-film form, suggesting that linear-shaped **2,6′:2′,6″-terazulene** molecules are closely packed in the solid film, with the intermolecular electronic interaction being strongly enhanced. The lowest transition energy ($E_{g\text{-}abs}$) in thin-film form was estimated to be 1.63 eV from the absorption edge (Figure 1B). It should be noted that **2,6′:2′,6″-terazulene** has a narrow band gap in spite of the absence of any electron donor or electron acceptor substituent. The highest occupied molecular orbital (HOMO) level determined by photoelectron yield spectroscopy (Figure S18 in SI) was −5.56 eV, and the lowest unoccupied molecular orbital (LUMO) level estimated from $E_{g\text{-}abs}$ and the HOMO level was −3.93 eV. The LUMO level of **2,6′:2′,6″-terazulene** was similar to that of C_{60} (−3.8 eV),[19] which is a common n-type semiconductor material. These findings indicate the material to be suitable for both hole- and electron-injection from an Au electrode with a Fermi level of −4.9 eV.

Single crystals of **2,6′:2′,6″-terazulene** grown by slow gradient sublimation showed a rigid and planar molecular structure (Figure 2A). As a result, 2,6-oligoazulenes, with an azulene unit connected at the 2,6-position, should exhibit less hindrance between adjacent azulene moieties. It therefore has the characteristics that are necessary to extend highly linear π-conjugated systems. The molecular long axes (*c*-axis) exhibited a lamellar structure (Figure 2B), which took the form of the well-defined herringbone arrangement generally observed in linear π-conjugated molecules, suitable for high mobility in OFETs (Figure 2C). Structural refinement yielded a global pseudosymmetry with a 1:1 disorder between the parallel and antiparallel orientations; the two molecules were geometrically equal (see the SI - Crystal Structure Determination).

Top-contact field-effect transistors were fabricated by vacuum deposition of **2,6′:2′,6″-terazulene** with an active layer thickness of 60 nm on a substrate of octadecyl trichlorosilane (ODTS)-treated Si/SiO_2. The source and drain electrodes were prepared by gold evaporation, with channel length and width of 50 μm and 5.5 mm, respectively. The FET devices were measured in a glovebox with nitrogen atmosphere. Output characteristics and transfer characteristics are shown in parts A and B of Figure 3, respectively. The drain

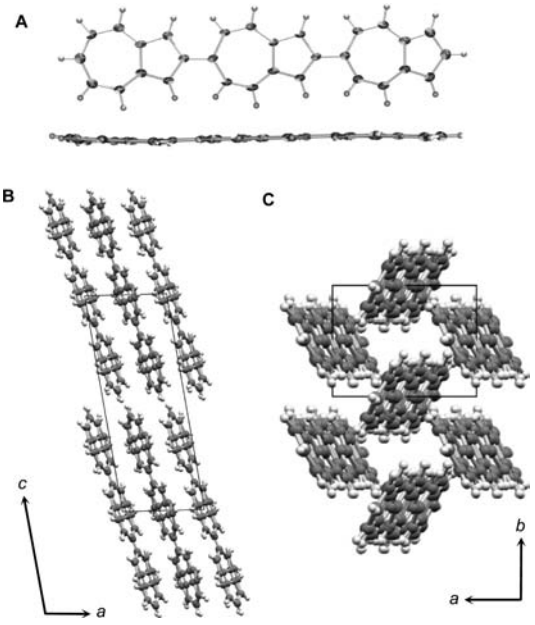

Figure 2. Crystal structure of 2,6′:2′,6″- terazulene: (A) Thermal ellipsoid drawing of top and side views at 50% probability level. (B) Partial view along the *b*-axis with clear indication of a layer structure along the *c*-axis. (C) Perspective view with clear indication of the herringbone packing.

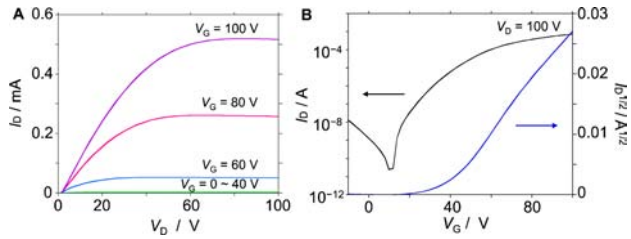

Figure 3. OFET characteristics of top-contact devices made of **2,6′:2′,6″-terazulene** at 100 °C: (A) Output curves at different gate voltages. (B) Transfer curves in the saturated region at a drain voltage of −100 V.

current (I_d) is increased at the positive gate voltage but not measurably so at the negative gate voltage. This striking result means that **2,6′:2′,6″-terazulene** acted as an n-type material OFET. The output curves of the device also showed good saturation behaviors (Figure 3A,B). The performance of the OFETs fabricated at different substrate temperatures (T_{sub}) is summarized in Table 1. The FET mobilities gradually improved

Table 1. OFET Characteristics of 2,6′:2′,6″-Terazulene

T_{sub} (°C)	μ_{FET} (cm^2 V^{-1} s^{-1})	I_{on}/I_{off}	V_{Th} (V)
RT	1.3×10^{-2}	3.9×10^5	26.1
60	0.10	3.7×10^6	30.6
100	0.29	2.5×10^7	37.1
140	3.0×10^{-2}	4.7×10^5	33.2

with increasing T_{sub}. The devices fabricated at T_{sub} = 100 °C demonstrated the highest performance, with a carrier mobility (μ_{FET}) of 0.29 cm^2 V^{-1} s^{-1}, and an on/off ratio (I_{on}/I_{off}) of 2.5×10^7. When T_{sub} reached 140 °C, OFET performance decreased.

dx.doi.org/10.1021/ja410696j | J. Am. Chem. Soc. 2013, 135, 19095−19098

To clarify the relationship between the thin-film structure and device performance, the former was analyzed by X-ray diffraction while the film morphology was studied by atomic force microscopy (AFM). X-ray diffraction measurements with an out-of-plane configuration of **2,6′:2′,6″-terazulene** gave a series of peaks assignable to (00*h*) reflections (Figure 4A). The

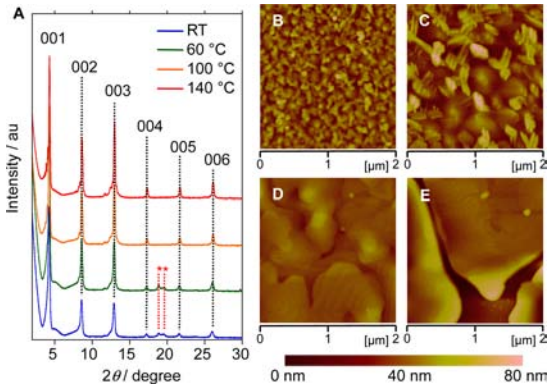

Figure 4. Thin film analysis: (A) Out-of-plane X-ray diffraction patterns of evaporated thin films of **2,6′:2′,6″-terazulene** on ODTS-treated Si/SiO_2 substrate; (B–E) AFM images of the **2,6′:2′,6″-terazulene** film for FET devices with top-contact configuration T_{sub} = RT (B), T_{sub} = 60 °C (C), T_{sub} = 100 °C (D), T_{sub} = 140 °C (E), respectively.

diffraction peak at 2θ = 4.29° corresponded to a *d*-spacing of 20.6 Å, in good agreement with the crystallographic *c*-axis length of the single crystal 20.6 Å. This indicated that the **2,6′:2′,6″-terazulene** molecules take the edge-on orientation in film form (Figure 4B). When the T_{sub} was lower than 60 °C, two weak peaks assignable to face-on orientation were observed, which would create the disadvantage of carrier passes parallel to the substrate.

The AFM images of the films at different T_{sub} are shown in B–E of Figure 4. The grain size on the substrate was largely influenced by T_{sub}; the size became progressively larger with increasing T_{sub} (Figure 4B,C). A highly regular terrace structure was observed at T_{sub} = 100 °C, where the step height of 20.5 Å corresponded to the *d*-spacing of *c*-axis (Figure 4D). This film structure is ideal for high FET mobility. Increasing the temperature further caused cracks on the film at T_{sub} = 140 °C (Figure 4E) that were detrimental to carrier mobility.

Thus, **2,6′:2′,6″-terazulene** gave a highly crystalline film and achieved n-type operation in OFET devices in spite of being a simple hydrocarbon molecule. These characteristic properties are derived from its unique electronic state that involves the intramolecular dipole moment of the azulene unit. We calculated the detailed electronic states of **2,6′:2′,6″-terazulene** using the DFT method at the B3LYP/6-31G(d)//B3LYP/6-31G(d) level. The calculated dipole moment was large, at 5.30 D, far exceeding 3 times the dipole of a single azulene unit (1.08 D): evidence of the concerted effect of three dipole moments in the same direction. The HOMO is significantly localized mainly in the five-membered ring at one end of the azulene moiety, whereas the LUMO are spread over the whole molecule, with a weak localization in the seven-membered ring (Figure 5A). This biased distribution of HOMO clearly affects the carrier transport property in OFET devices. As seen in Figure 5B, when the molecules took an antiparallel orientation, the HOMO could not overlap adjacent molecules due to

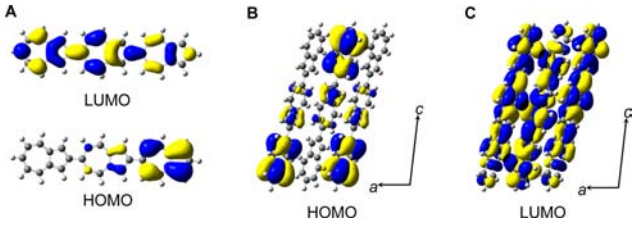

Figure 5. Crystal structure and packing structure with calculated frontier orbitals of **2,6′:2′,6″-terazulene**: (A) Calculated frontier orbitals at the B3LYP/6-31G(d)//B3LYP/6-31G(d) level. (B) Partial view along the *b*-axis with HOMO orbitals; (C) Partial view along the *b*-axis with LUMO orbitals.

HOMO localization at the edge of the molecule. As a result, hole transport through the crystal is naturally prevented. In contrast, the LUMO could overlap adjacent molecules (Figure 5C). This is the reason why **2,6′:2′,6″-terazulene** showed n-type operation in the OFET device.

To estimate the carrier transport potential quantitatively, we evaluated their intermolecular electronic coupling constants. The calculated electronic coupling constants in each direction are shown in Figure S17 (SI). The LUMO had a higher electronic coupling constant in almost all directions than those of the HOMO (see SI - Transfer Integrals-Determination). This trend was typically observed in the antiparallel orientation. Therefore, if the film was composed of a mixture of parallel and antiparallel couplings, as indicated by single-crystal XRD data, the weak coupling of the antiparallel orientation in HOMO would determine the total hole mobility. We also evaluated their reorganization energies. Those values were 0.101 eV for hole transport, and 0.183 eV for electron transport, respectively (see SI - Reorganization Energies-Determination). A higher reorganization energy is disadvantageous to carrier transport. Therefore, the n-type operation should be explained by the orbital distribution, not by the reorganization energy.

This unique asymmetry between HOMO and LUMO is interpreted as follows. The azulene unit has a characteristic HOMO distribution in which there is no orbital density at the 2 and 6 positions, derived from its nonalternant hydrocarbon character. The three highest orbitals in terazulene generated from three azulene HOMOs therefore closely reflect the distribution of a single azulene unit due to weak conjugation (see SI – Molecular Orbitals Distribution and Energy Levels). If there were absolutely no conjugation, these three orbitals would degenerate and equally contribute to charge transport, which cannot explain the absence of p-type operation. However, terazulene has a large dipole moment of 5.30 D, which forms an electrostatic potential gradient inside the molecule and resolves the degeneracy (energy split between HOMO and HOMO−1 is calculated to be 0.29 eV). Thus, the orbital with a large amplitude on the negative-side azulene unit is destabilized by the dipole and becomes HOMO contributing to carrier transport, as shown in Figure 5A. In contrast, since the LUMO of azulene has sufficient amplitude at the 2- and 6-positions, three LUMOs of azulene are strongly conjugated in terazulene and generate three unoccupied orbitals with large energy splits. As a result, the LUMO of terazulene has a uniform, well-spread distribution through the molecule, achieving high orbital overlapping and high electron mobility. This asymmetric property between HOMO and LUMO in terazulene is derived from the asymmetric character of HOMO and LUMO in azulene, a nonalternant hydrocarbon compound.

dx.doi.org/10.1021/ja410696j | J. Am. Chem. Soc. 2013, 135, 19095–19098

Since conventional alternant hydrocarbon compounds used as organic semiconductors have strong conjugation for both HOMO and LUMO, it is difficult to obtain an extremely biased distribution, even in a push−pull system with electron-donating and -withdrawing groups. In addition, HOMO and LUMO have oppositely biased distributions.

The appearance of n-type semiconductor behavior in **2,6′:2′,6″-terazulene** is the first instance wherein this unique electronic state of azulene has been exploited. This concept, molecular orbital distribution control, gives a new strategy for controlling polarity of organic semiconductors.

■ ASSOCIATED CONTENT

Ⓢ Supporting Information

^{1}H and ^{13}C NMR and HRMS data for all new compounds, MO calculation details, and X-ray crystallographic data; crystallographic files (cif). This material is available free of charge via the Internet at http://pubs.acs.org.

■ AUTHOR INFORMATION

Corresponding Authors

nakayama@yz.yamagata-u.ac.jp
kgri7078@yz.yamagata-u.ac.jp

Notes

The authors declare no competing financial interest.

■ ACKNOWLEDGMENTS

This work was supported by a Grant-in-Aid for Young Scientist (B) (25870076 to H.K.) from the Ministry of Education, Culture, Sports, Science and Technology (MEXT).

■ REFERENCES

(1) Lemal, D. M.; Goldman, G. D. *J. Chem. Educ.* **1988**, *65*, 923−925.
(2) Michl, J.; Thulstrup, E. W. *Tetrahedron* **1976**, *32*, 205−209.
(3) Wang, F. K.; Lai, Y. H.; Kocherginsky, N. M.; Kosteski, Y. Y. *Org. Lett.* **2003**, *5*, 995−998.
(4) Wang, F. K.; Lai, Y. H.; Han, M. Y. *Macromolecules* **2004**, *37*, 3222−3230.
(5) Ito, S.; Kubo, T.; Morita, N.; Ikoma, T.; Tero-Kubota, S.; Tajiri, A. *J. Org. Chem.* **2003**, *68*, 9753−9762.
(6) Wang, X. B.; Ng, J. K. P.; Jia, P. T.; Lin, T. T.; Cho, C. M.; Xu, J. W.; Lu, X. H.; He, C. B. *Macromolecules* **2009**, *42*, 5534−5544.
(7) Amir, E.; Amir, R. J.; Campos, L. M.; Hawker, C. J. *J. Am. Chem. Soc.* **2011**, *133*, 10046−10049.
(8) Zielinski, T.; Kedziorek, M.; Jurczak, J. *Chem.—Eur. J.* **2008**, *14*, 838−846.
(9) Kurotobi, K.; Kim, K. S.; Noh, S. B.; Kim, D.; Osuka, A. *Angew. Chem., Int. Ed.* **2006**, *45*, 3944−3947.
(10) Smits, E. C. P.; Setayesh, S.; Anthopoulos, T. D.; Buechel, M.; Nijssen, W.; Coehoorn, R.; Blom, P. W. M.; de Boer, B.; de Leeuw, D. M. *Adv. Mater.* **2007**, *19*, 734−738.
(11) Muranaka, A.; Yonehara, M.; Uchiyama, M. *J. Am. Chem. Soc.* **2010**, *132*, 7844−7845.
(12) Mei, J.; Diao, Y.; Appleton, A. L.; Fang, L.; Bao, Z. *J. Am. Chem. Soc.* **2013**, *135*, 6724−6746.
(13) Yamaguchi, Y.; Maruya, Y.; Katagiri, H.; Nakayama, K.; Ohba, Y. *Org. Lett.* **2012**, *14*, 2316−2319.
(14) Kurotobi, K.; Tabata, H.; Miyauchi, M.; Murafuji, T.; Sugihara, Y. *Synthesis* **2002**, 1013−1016.
(15) Ito, S.; Nomura, A.; Morita, N.; Kabuto, C.; Kobayashi, H.; Maejima, S.; Fujimori, K.; Yasunami, M. *J. Org. Chem.* **2002**, *67*, 7295−7302.
(16) Nozoe, T.; Seto, S.; Matsumura, S. *Bull. Chem. Soc. Jpn.* **1962**, *35*, 1990−1998.
(17) Ito, S.; Kubo, T.; Morita, N.; Matsui, Y.; Watanabe, T.; Ohta, A.; Fujimori, K.; Murafuji, T.; Sugihara, Y.; Tajiri, A. *Tetrahedron Lett.* **2004**, *45*, 2891−2894.
(18) Watanabe, M.; Chang, Y. J.; Liu, S. W.; Chao, T. H.; Goto, K.; Islam, M. M.; Yuan, C. H.; Tao, Y. T.; Shinmyozu, T.; Chow, T. J. *Nat. Chem.* **2012**, *4*, 574−578.
(19) Schulze, K.; Uhrich, C.; Schueppel, R.; Leo, K.; Pfeiffer, M.; Brier, E.; Reinold, E.; Baeuerle, P. *Adv. Mater.* **2006**, *18*, 2872−2875.